Localized Preheating Approaches for Reducing Residual Stress in Additive Manufacturing

Pruk Aggarangsi and Jack L. Beuth
Department of Mechanical Engineering
Carnegie Mellon University
Pittsburgh, PA

Abstract

Uniform preheating can be used to limit residual stress in the solid freeform fabrication of relatively small parts. However, in additive manufacturing processes, where a feature is deposited onto a much larger part, uniform preheating of the entire assembly is typically not practical. This paper considers localized preheating to reduce residual stresses, building on previous work using a defined thermal gradient through the part depth as a metric for predicting maximum final residual stress. The building of thin-walled structures is considered. Two types of localized preheating approaches are compared, appropriate for use in laser- or electron beam-based additive manufacturing processes. In evaluating the effectiveness of each approach, a simplified thermomechanical model is used that can be related directly to analytical thermomechanical models for thermal stresses in unconstrained thin plates. Results are presented showing that one of the methods yields temperature profiles likely to yield reduced residual stresses at room temperature. Mechanical model results confirm this, showing a significant reduction in maximum stress values. A more complete thermomechanical simulation of thin wall fabrication is used to verify the trends seen in the simplified model results.

Introduction

In this paper, Additive Manufacturing (AM) refers to electron beam, laser or other molten metal deposition processes used to add complex features to larger structures, or to repair worn components. This class of manufacturing processes has evolved from solid freeform fabrication (SFF) techniques and the most progress to date has been made in developing laser beam-based processes, (e.g. Directed Light Fabrication, LENS® and Direct Metal Deposition to name just a few [1-2]). Electron beam-based processes, though more complicated to use, offer unique advantages in thermal control of the melt pool area compared to analogous laser-based processes [3]. At this time, AM methods are serious candidates for the fabrication and repair of a range of high-value-added components and are receiving significant attention in the aerospace industry. Applications include the addition of features to engine casings, as one step in a low-cost manufacturing process, and the repair of worn turbine blade tips, either on individual blades or integral bladed disk (blisk) designs.

Residual stress is an inherent part of additive manufacturing, and the goal of strategies to control stress is to reduce its magnitude to a manageable level. In most cases, fabricated parts or features are heat treated after deposition to relieve stress. As a result, in most cases stress-induced distortion during deposition is the principal concern (as opposed to high stresses leading to premature failure during use).

Previous work by the authors and their co-authors has addressed the modeling and measurement of residual stress in metal and polymer deposition SFF processes [4-7]. Control of melt pool size under steady-state conditions has been considered by using a process map approach to plot melt pool size over the full range of process variables for LENS® [8-11]. The process map approach has been extended to consider melt pool size control under transient conditions and as a function of process size scale [12-15]. The issue of residual stress control has also been addressed using a process map approach [16, 17]. In that work, a defined thermal gradient behind the melt pool is proposed as a means for predicting reductions in final magnitudes of residual stress based on thermal simulation results. It is shown that the gradient does correlate with maximum residual stress magnitudes over the full practical range of laser powers and velocities. A process map of the thermal gradient as a function of process variables is also presented, valid for deposition of 304 stainless steel by a LENS® – scale laser-based process. Important conclusions of that work are that uniform preheating is a practical means of limiting residual stress magnitudes and melt pool size increases caused by preheating can easily be corrected by decreased laser power and/or increased laser velocity.

Because additive manufacturing processes involve the deposition of features onto large parts, uniform preheating of the entire assembly is, if possible, inefficient and expensive. In this paper, knowledge of the role of thermal gradients in determining residual stress is used to consider localized preheating of deposited features as a means to limit final stress magnitudes. In the next section, an overview of fundamental analytical concepts for thermal stresses in thin plates is given, along with a review of the key results from Vasinonta, et al. [16, 17]. Two types of strategies for altering temperatures near the surface of a thin wall are then considered, using a simplified thermomechanical model that has mechanical boundary conditions like those of existing analytical models. This allows a direct link to be made between trends in results seen in the simulations of additive manufacturing and analogous analytical models. Finally, results from a more realistic (and time-consuming) 3-D thermomechanical model are presented to determine if successful strategies identified using the simplified models are likely to hold for the deposition of thin-walled structures by additive manufacturing.

Analytical Solution and Existing Work

Analytical Solution

A one-dimensional elastic thermal stress solution for the stresses in an unconstrained plate is presented by Boley and Weiner [18]. The plate has a depth dimension (in the z direction) of h and is assumed to be long in the x direction, with results independent of the x coordinate. The solution is also independent of the thickness (y) coordinate, and this dimension is assumed small so that a condition of plane stress exists. The single stress in this plate is σ_{xx} and the equation for it is given by

$$\sigma_{xx} = \alpha E \left\{ -T + \frac{1}{2h} \int_0^h T \, dz + \frac{3z}{2h^3} \int_0^h Tz \, dz \right\} \quad (1)$$

In eq. (1), T is T(z) the distribution of temperature through the depth of the plate, with an assumption of no dependence on the x (length) or y (thickness) coordinates.

Although this analytical solution is for a geometry somewhat similar to a thin-walled feature, it is for highly idealized conditions. Compared to additive manufacturing of a thin-walled feature, this solution includes no plasticity, no constraint from the base component on the base of the thin wall, and neglects the travel of the heat source across the top of the wall. However, this solution can provide insights into the relationships between temperature and stress distributions for additive manufacturing applications. For example, the stress distributions of the above equation corresponding to cooling to room temperature from three different temperature profiles with top surface temperature T_{top} = 1150 K are plotted in Figure 1. In each case, it is assumed that the plate is initially stress-free. The value of T_{top} = 1150 K is used because of its choice by Vasinonta, et al. [16, 17] to represent the relationship between temperature distributions and maximum residual stress in the deposition of 304 stainless steel by the LENS® process (details to be provided in the next subsection).
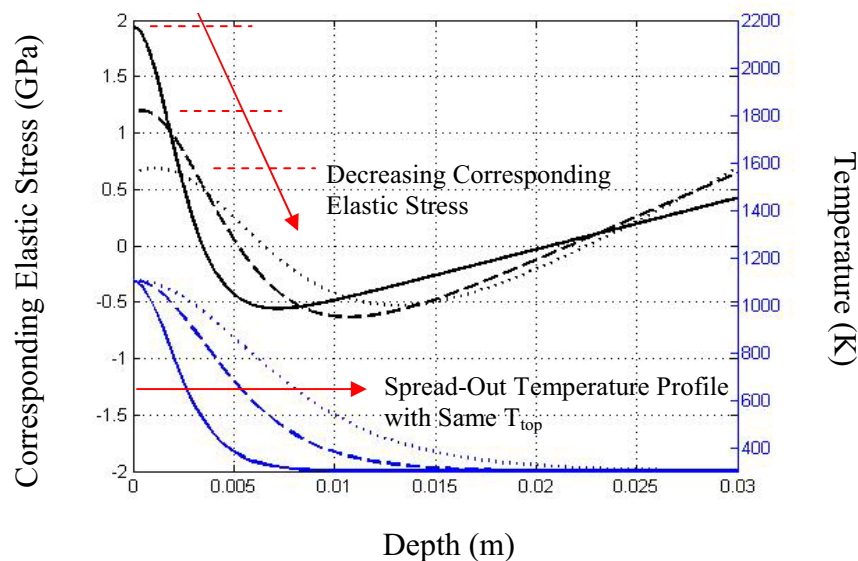

Figure 1 Comparison of 1-dimensional elastic analytical stress solution results for three temperature profiles T(z).

As can be seen in Fig. 1, temperature distributions with elevated temperatures more concentrated near the top of the thin plate yield larger stresses upon cooling to room temperature. This is because in these cases, thermal contractions in the top portion of the plate are more constrained by the remainder of the plate, which contracts less. This simple example suggests that maximum stress values can be tied to the thermal gradient $\dfrac{dT}{dz}$ in the region near the top of the thin plate. Large values of $\dfrac{dT}{dz}$ yield large residual stresses at room temperature.

Existing Work for Additive Manufacturing Processes

The concept of using a defined thermal gradient near the top surface as a metric for predicting maximum residual stress magnitudes has been applied by Vasinonta et al. [16, 17]. In that work, it is recognized that temperature distributions behind the melt pool look very similar to those shown in Fig. 1. It is also recognized that for SS 304,

significant stress build-up does not occur until the top surface temperature equals 1150 K or less. Thus, trends in maximum stress values after cool-down to room temperature in simulations of a heat source moving across the top of a thin-walled structure are compared to trends in thermal gradients, measured at a distance behind the melt pool where the temperature on the top surface equals 1150 K, and at a nondimensional depth such that the T(z) distribution is nearly linear. Results for this defined thermal gradient are plotted over the full range of process variables for the LENS® process (operating with a maximum laser power of 470 W). Figure 2 gives a summary plot of how maximum stresses compare to this defined thermal gradient behind the melt pool.
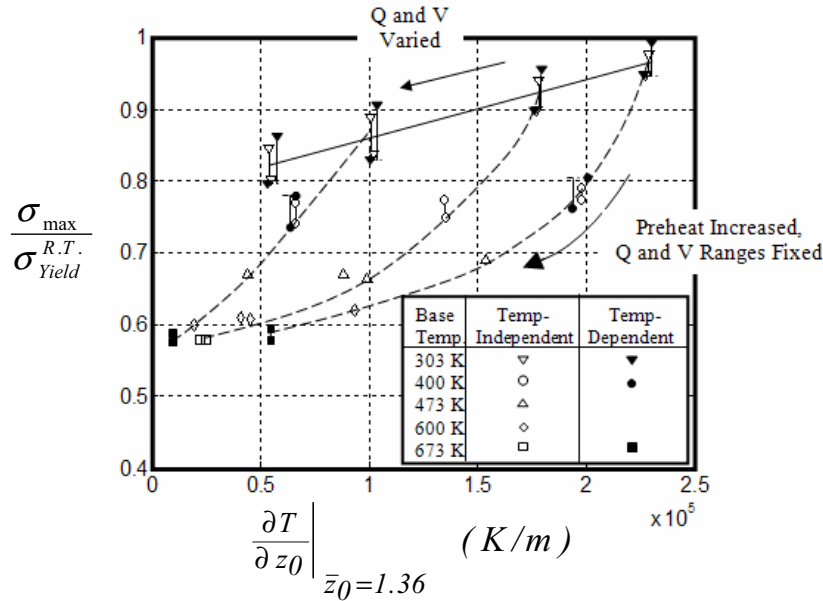

Figure 2 Relationship between a defined temperature gradient behind the melt pool and the magnitude of maximum residual stress (Vasinonta, et al. [17]).

Figure 2 from the work by Vasinonta et al. [17] reveals the relationship between the defined thermal gradient behind the melt pool and the magnitude of maximum residual stress (in the x direction) in a tall wall after the wall is cooled down to room temperature. Maximum stress values are normalized by the axial yield stress at room temperature, $\sigma_{Yield}^{R.T.}$. The straight solid line in Figure 2 shows the trend in stress reduction by manipulating laser power and velocity only. For most combinations of laser power and velocity, thermal gradients are high and the maximum stress equals the yield stress (the model used assumes perfect plasticity). These cases are not shown in Fig. 2. However, Fig. 2 does show that some combinations of laser power and velocity can result in maximum stresses below the room temperature yield stress. Furthermore, points on the solid line for a fixed value of thermal gradient cover the full range of laser power and velocity. The result is little change in maximum stress, indicating that the defined thermal gradient is correlated with final maximum residual stress.

The dashed curves in Fig. 2 are for cases with the same power and velocity values used for data on the solid line, but with a uniform preheat added. In these cases of part preheating, in addition to the benefit of a lower temperature gradient, a further reduction in the magnitude of residual stress is observed. This is due to the lowered value of yield

stress at the preheat temperature limiting the magnitude of the maximum stress. The conclusion of this work is that uniform preheating introduces two mechanisms for stress reduction: decreasing the temperature gradient and limiting the magnitude of stress to the yield stress at elevated temperature. Furthermore, it is shown that melt pool size increases induced by uniform preheating can easily be eliminated by minor reductions in laser power and/or increases in laser velocity.

Localized Preheating to Reduce Residual Stress

In the additive manufacturing of features onto a large part, or in the solid freeform fabrication of large components, uniform preheating may be impractical or impossible. In this study, existing work relating thermal gradients to residual stress is used as a foundation for considering localized, near-surface preheating as a means for limiting residual stress. Two types of localized preheating methods are considered, as illustrated in Fig. 3. The first method involves use of a second, lower-power heat source, either ahead of or behind the melt pool (see Fig. 3a). The second method involves preheating of the top surface to a prescribed top surface temperature. In this case, it is assumed that a steady-state is reached, such that the temperature distribution between the top surface and the base of the thin wall (with a fixed temperature $T_{base} = 303$ K) is linear.
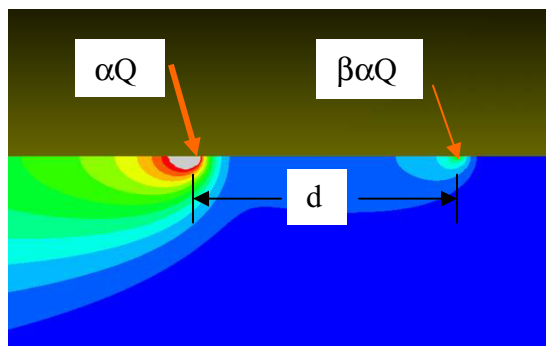

Figure 3-a Schematic illustration of feature deposition with an additional heat flux leading the primary heat flux.
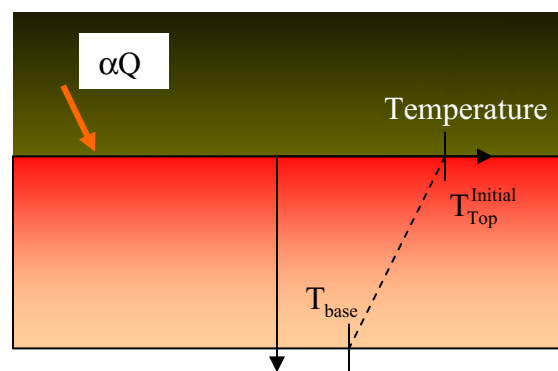
Figure 3-b Schematic illustration of feature deposition on a part preheated to a linear temperature profile thorough the part depth.

In laser-based processes, application of a secondary heat source ahead of or behind the melt pool could be accomplished by adding a second controlled laser source to the system, or perhaps by splitting the beam of a single laser. In electron beam-based processes, it is possible to move the beam at very high rates, so that a single beam could be moved back and forth between the melt pool and the regions ahead of or behind it. Models of additional heat sources described herein can also be considered as special cases of general approaches of heating ahead of the main power source and heating behind it. Preheating of the top surface of the part is a method often used in electron beam-based processes, where the beam is rapidly moved in a raster pattern across the top of the part before deposition is initiated. In laser-based processes, this approach could be pursued with a low-power, defocused beam. Uniform top surface preheating can also be considered as a second general approach to surface heating in addition to heating ahead of or behind the melt pool.

713

Numerical Models and Material Properties

In this work the commercial finite element package ABAQUS has been used to perform numerical simulations. Two types of models, simplified models and more complete models, are used to serve two different purposes. The simplified numerical models are used to quickly evaluate localized preheating approaches. By neglecting the effect of mechanical constraints at the base of the thin wall, simplified model results can also be related to those from the existing elastic stress solution described in the previous section [18]. The simplified model consists of uncoupled two-dimensional thermal and mechanical models, having identical geometries and mesh resolution. Schematics of the models and their boundary conditions are shown in Figure 4a and 4b. The length and height, designated as L and h, are 50 mm and 30 mm, respectively, which are representative dimensions for a small-scale thin-walled feature. The length L of 50 mm is large enough to ensure steady state thermal and mechanical conditions in the area near the center of the feature where numerical data is extracted. The height h of 30 mm is also large enough for the feature to behave like a tall wall in the thermal simulations, where the thermal condition at the base has a minimal effect on the temperature field near the melt pool [8-10].
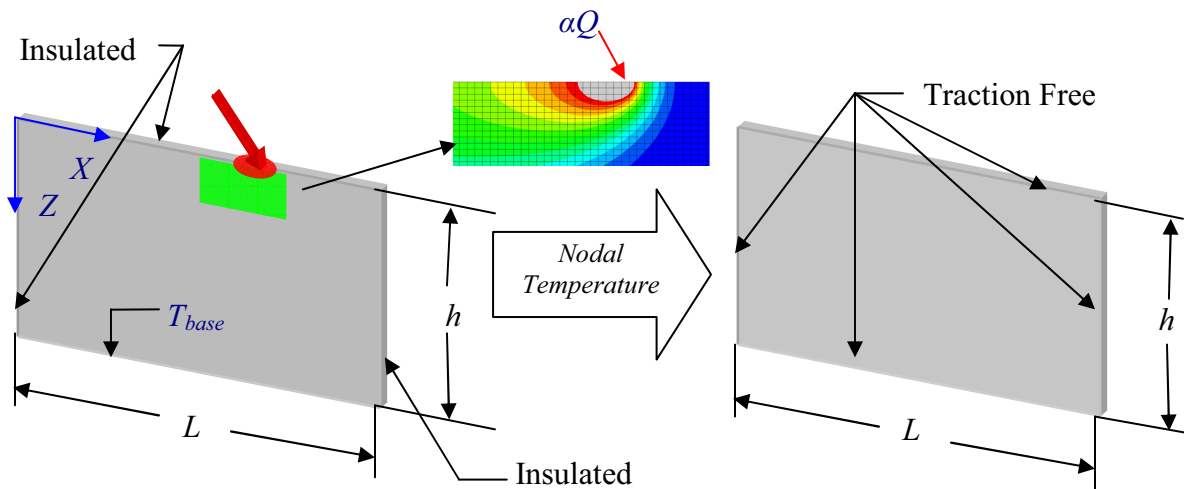

Figure 4a Illustration of the simplified thermal finite element model and its boundary conditions.

Figure 4b Illustration of the simplified mechanical finite element model and its boundary conditions.

A uniform mesh resolution is used in the simplified models. The absorbed laser power, designated by αQ, is applied as a concentrated nodal heat flux. A moving heat flux is simulated by moving the point source by one nodal spacing in each time step. The history of the temperature field for each time step is recorded and exported as a direct input to the mechanical model. In the simplified thermal models, heat convection and radiation to the surroundings are neglected as well as heat released by evaporation. Compared to conduction, each of these heat transfer mechanisms are minor contributors to cooling of the melt pool [20]. The temperature at the base is fixed at T_{base} to simulate the deposition of a feature onto a large part acting as a heat sink. The simplified mechanical models assume traction-free conditions on all external surfaces (matching boundary conditions in the analytical model of Boley and Weiner [18]) and neglect strain hardening. In all cases

considered, an absorbed laser power $\alpha Q = 105$ W, laser velocity $V = 7.62$ mm/s and wall thickness of 1.3 mm are used, consistent with previous work by Vasinonta et al. [8-10, 16, 17]. In all cases, a single pass of the heat source across the top of the wall is simulated, followed by cooling to an ambient temperature of 303 K.

More complete numerical models have also been used to simulate thin wall stress build-up. Uncoupled three-dimensional 8-noded thermal and mechanical solid elements have been used to simulate a thin-walled feature having identical dimensions to those of the simplified models. More representative boundary conditions are assigned to both the thermal and mechanical models. A schematic illustration of the mesh and prescribed conditions of the more complete models is shown in Figure 5. For both thermal and mechanical models, a thin-walled feature of half the thickness of the actual feature (6.5 mm) is used with symmetry conditions imposed on the X-Z plane. Instead of the concentrated heat flux applied at each node in the simplified model, a more realistic uniformly distributed heat flux is applied over 0.5 mm along the X-axis in a step-by-step fashion. Boundary conditions in the thermal model include forced heat convection on the top surface, natural heat convection on other free faces and heat radiation on all open surfaces. Important characteristics of the more complete mechanical model are constrained conditions at the model base and the modeling of temperature-dependent strain hardening.

Side	Thermal Conditions
1	Fixed Temperature $T = T_{base}$
2	Symmetry (i.e. Insulated)
3	Forced Convection h = 10 W/m²K Radiation $\varepsilon = 0.4$
4,5	Natural Convection h = 5 W/m²K Radiation $\varepsilon = 0.4$

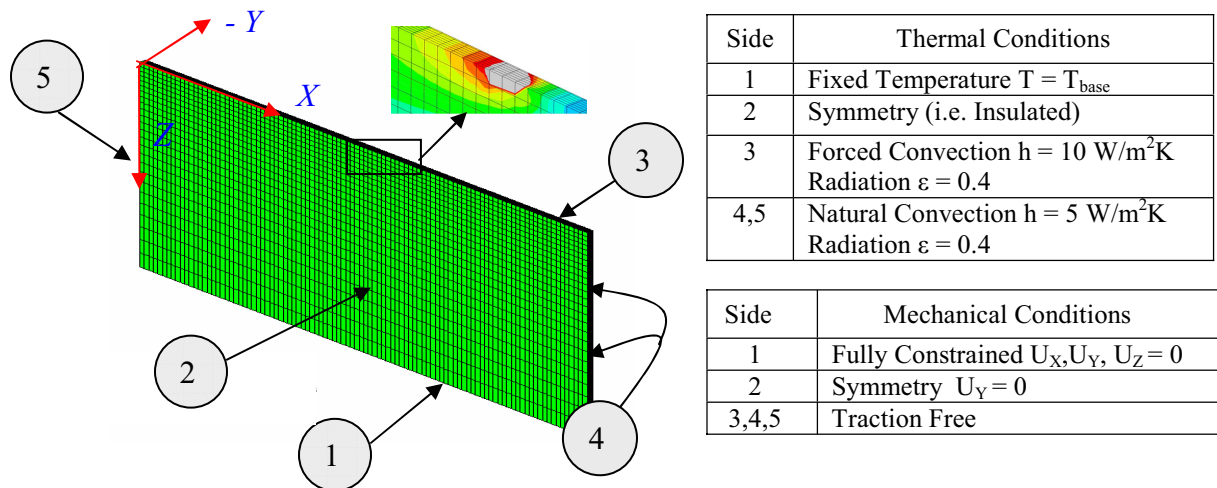| Side	Mechanical Conditions
1	Fully Constrained $U_X, U_Y, U_Z = 0$
2	Symmetry $U_Y = 0$
3,4,5	Traction Free

Figure 5 Schematic illustration of the more complete model and its boundary conditions

Thermal and mechanical properties of AISI 304 stainless steel are obtained from Dobranich and Dykhuizen [20] and Peckner and Bernstein [19]. Temperature-dependent properties used in both the simplified and more complete models include heat conduction, specific heat, coefficient of thermal expansion, Young's modulus and yield stress. The latent heat of fusion is also included in both model types. The heat convection coefficient (h) and radiation constant (ε) used in the more complete models are taken from Dobranich and Dykhuizen [20]. Temperature-dependent yield stress values used in both model types are taken from Peckner and Bernstein [19]. Strain hardening behavior used in the more complete mechanical models is extrapolated from an existing stress-strain curve [21] and the available temperature-dependent yield stress data.

Numerical Results

Localized Temperature Manipulation by Use of an Additional Heat Flux

Simulations of an additional heat flux have been carried out with the goal of locally activating one or both mechanisms of stress reduction described in the section on existing work [16, 17]. Many combinations of the power fraction (β) and the distance from the primary heat flux in multiples of the melt pool length have been simulated, but only two representative cases are presented herein. Temperature data are extracted from nodes along the center line of the thin wall (i.e. along x = 25 mm) from the time step having the top surface temperature (T_{top}) equal to a designated value.

Temperature distributions with T_{top} = 900 K and T_{top} = 675 K for cases with β = 0.40 and the secondary heat flux 10 melt pool lengths ahead of or 20 melt pool lengths behind the primary heat flux are shown in Figure 6. Both cases are compared to the "ambient case" of a single heat flux with αQ = 105 W. Temperature distributions for the two cases having an additional heat flux are similar to each other. For the case of T_{top} = 673 K they are indistinguishable. Although temperatures for both cases of an additional heat flux are noticeably different than those for the ambient case, the differences are not large.
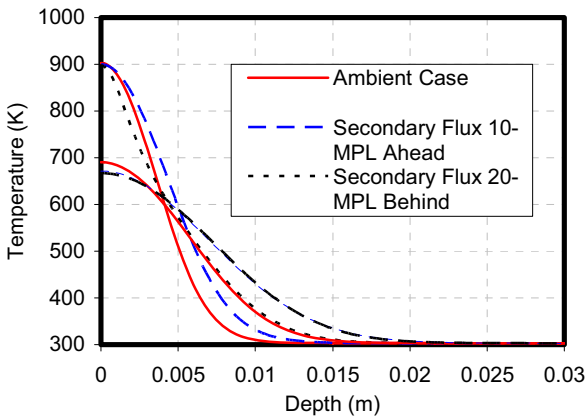
Figure 6 Temperature distributions for feature deposition under ambient conditions and for cases with an additional heat flux leading or following the primary heat flux.
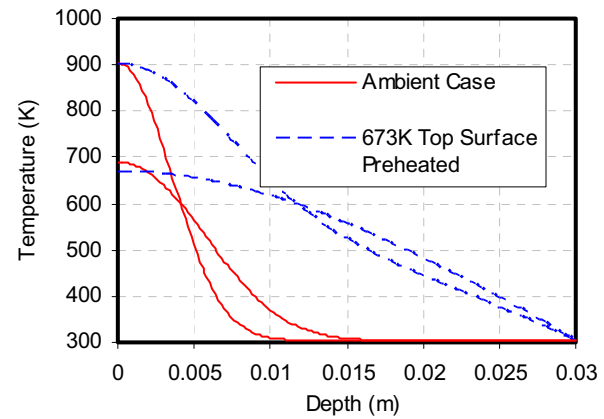
Figure 7 Temperature distributions for feature deposition under ambient conditions and for the case of a part preheated to a linear temperature distribution through its depth.

Residual stress distributions resulting from the temperatures plotted in Fig. 6 are plotted in Fig. 8, where stress values are also taken from the path along the center line of the thin wall. The magnitude of residual stress is presented as a fraction of the yield stress at room temperature (σ_y^{RT}). For both cases, the use of an additional heat source has changed the stress distributions only slightly. The maximum residual stress has been reduced, but the reduction is small. This slight decrease in maximum residual stress is consistent with the trends seen in the temperature distributions.

Localized Temperature Manipulation by Uniform Preheating of the Deposition Surface

Simulation of uniform top surface preheating is performed by applying a constant temperature T_{top} to the top surface of the thin-walled feature. This boundary condition is applied until a steady state is achieved and the temperature distribution through the wall depth is linear, (with a minimum value of T_{base} at the base of the wall). The top surface temperature condition is then removed and simulation of a single pass of a 105 W heat source across the top of the wall is immediately initiated. As with the use of an additional heat flux, this approach is meant to directly reduce temperature gradients as well as apply part preheating near the top surface of the thin wall, which is where large tensile stresses develop.

Temperature distributions for deposition under ambient conditions and for the case of the top surface preheated to 673 K are shown in Figure 7. Clearly, the case of a 673 K preheated top surface shows considerably lower thermal gradients for both top surface temperatures of 900 K and 675 K. As illustrated in Figure 8 the final stress distribution is also significantly changed, with an approximately 18% reduction in maximum stress.
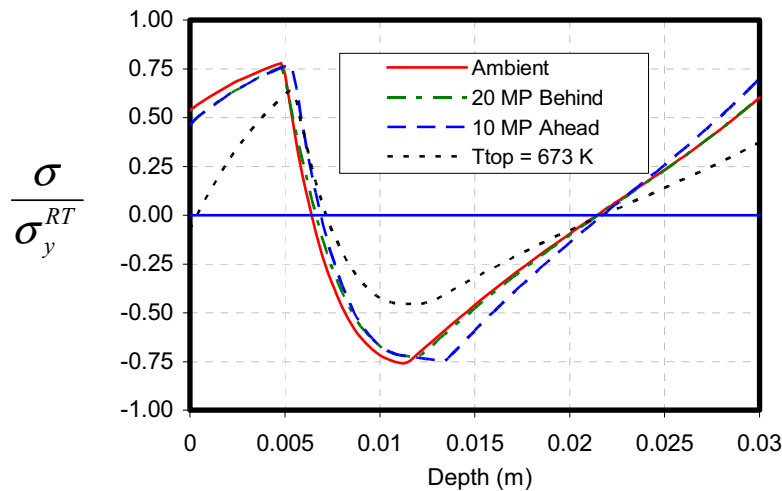

Figure 8 Comparison of final residual stress for deposition under ambient conditions with cases having an additional heat flux or a preheated top surface.

A More Complete Model of Thin Wall Deposition

Results from the simplified thermomechanical models suggest that the use of uniform top surface preheating can significantly alter temperature distributions through the wall depth, and correspondingly reduce maximum residual stresses present after the wall cools to a uniform temperature. More complete models have been used to further investigate this approach, where the most important added effect is that of constraint at the base of the wall. Also, because of the inclusion of strain hardening in the models, residual stresses can now be larger than the yield stress at room temperature.

Figure 9 shows a comparison between residual stress distributions for a single pass across the top of the wall under ambient conditions and for the case of top surface preheating to 673 K. The stress distributions through the depth of the models are very different from those of the simplified models. Because of hardening, maximum stresses

now occur at the very top of the wall, where maximum plastic straining occurs. At the base of the wall, stresses are negligible, due to the constraint imposed there. However, consistent with the simplified model results, a significant reduction in maximum residual stress (by a factor of approximately 1/3) is seen for the top surface preheating case. Thus the simplified models (whose results are more easily interpreted in the context of analytical solutions) are useful in identifying effective localized preheating approaches. Also, the approach of uniform top surface preheating appears effective in reducing maximum stress magnitudes.
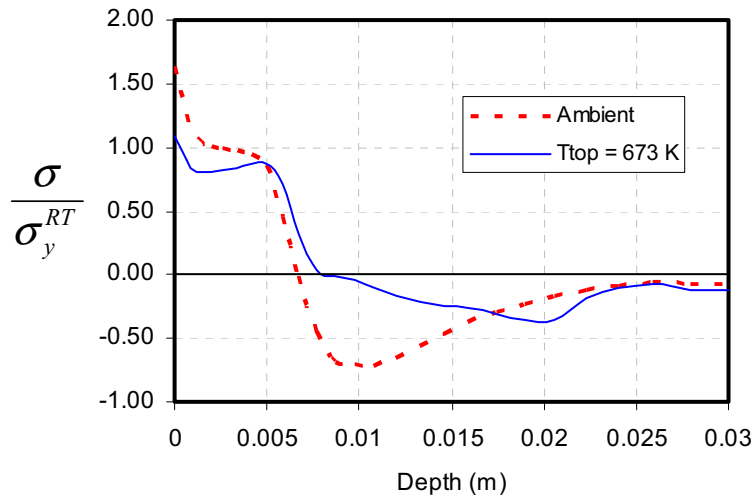

Figure 9 Final residual stress distributions obtained from a more complete model of thin wall deposition.

Conclusions

In this work, two localized preheating approaches are modeled for the additive manufacturing of thin-walled features: use of an additional heat flux ahead of or behind the melt pool and applying uniform preheating to the deposition surface. These approaches could be applied to laser- or electron beam-based processes. Comparisons are made using simplified models of a heat source moving across an unconstrained plate. This has allowed direct comparisons to be made with analogous analytical solutions from the literature. Model results show that temperature profiles are strong indicators of the magnitude of final maximum residual stress, and that a thermal gradient behind the melt pool can be used as a metric for determining which approaches will reduce residual stress the most. This is consistent with previous work by the authors and their co-authors.

Both cases of additional heat fluxes (leading or following the primary heat flux) result in minimal changes in temperature distributions as material cools behind the melt pool. Model results show noticeable but minor reductions in temperature gradient and maximum residual stress. On the other hand, applying a uniform preheat to the deposition surface results in significant changes in temperature distributions and residual stress. Simplified models show an approximately 18% reduction in maximum stress for the case where the top surface is heated to 673 K prior to the deposition. More complete simulations of the additive manufacturing process, taking into account constraint by the base structure, additional heat transfer mechanisms, strain hardening and 3-D effects show

the same trends seen in the simplified model results, with stress reductions as large as a factor of 1/3.

References:

1. Lewis, G.K. and Schlienger, E., "Practical Considerations and Capabilities for Laser Assisted Direct Metal Deposition," *Materials and Design*, Vol. 21, No. 4, 2000, pp. 417-423.

2. Mazumder, J., Schifferer, A., and Choi, J., "Direct Materials Deposition: Designed Macro and Microstructure," *Materials Research Innovations*, Vol. 3, No. 3, 1999, pp. 118-131.

3. Watson, J.K., Taminger, K.M., Hafley, R.A. and Petersen, D.D., "Development of a Prototype Low-Voltage Electron Beam Freeform Fabrication System," *Solid Freeform Fabrication Proceedings* (D.L. Bourell, J.J. Beaman, R.H. Crawford, H.L. Marcus and J.W. Barlow, eds.), Proc. 2002 Solid Freeform Fabrication Symposium, Austin, August 2002, pp. 458-465.

4. Klingbeil, N.W., Zinn, J.W. and Beuth, J.L., "Measurement of Residual Stresses in Parts Created by Shape Deposition Manufacturing," *Solid Freeform Fabrication Proceedings* (D.L. Bourell, J.J. Beaman, R.H. Crawford, H.L. Marcus and J.W. Barlow, eds.), Proc. 1997 Solid Freeform Fabrication Symposium, Austin, August 1997, pp. 125-132.

5. Klingbeil, N.W., Beuth, J.L., Chin, R.K, and Amon, C.H., "Measurement and Modeling of Residual Stress-Induced Warping in Direct Metal Deposition Processes," *Solid Freeform Fabrication Proceedings* (D.L. Bourell, J.J. Beaman, R.H. Crawford, H.L. Marcus and J.W. Barlow, eds.), Proc. 1998 Solid Freeform Fabrication Symposium, Austin, August 1998, pp. 367-374.

6. Ong, R., Beuth, J.L. and Weiss, L.E., "Residual Stress Control Issues for Thermal Deposition of Polymers in SFF Processes," *Solid Freeform Fabrication Proceedings* (D.L. Bourell, J.J. Beaman, R.H. Crawford, H.L. Marcus and J.W. Barlow, eds.), Proc. 2000 Solid Freeform Fabrication Symposium, Austin, August 2000, pp. 209-218.

7. Klingbeil, N.W., Beuth, J.L., Chin, R.K. and Amon, C.H., "Residual Stress-Induced Warping in Direct Metal Solid Freeform Fabrication," *International Journal of Mechanical Sciences,* Vol. 44, 2002, pp. 57-77. .

8. Vasinonta, A., Beuth, J.L. and Griffith, M.L., "Process Maps for Laser Deposition of Thin-Walled Structures," *Solid Freeform Fabrication Proceedings* (D.L. Bourell, J.J. Beaman, R.H. Crawford, H.L. Marcus and J.W. Barlow, eds.) Proc. 1999 Solid Freeform Fabrication Symposium, Austin, August 1999, pp. 383-391.

9. Vasinonta, A., Beuth, J.L., and Ong, R., "Melt Pool Size Control in Thin-Walled and Bulky Parts via Process Maps," *Solid Freeform Fabrication Proceedings* (D.L. Bourell, J.J. Beaman, R.H. Crawford, H.L. Marcus, K.L. Wood and J.W. Barlow, eds.), Proc. 2001 Solid Freeform Fabrication Symposium, Austin, August 2001, pp. 432-440.

10. Vasinonta, A., Beuth, J.L. and Griffith, M.L., "A Process Map for Consistent Build Conditions in the Solid Freeform Fabrication of Thin-Walled Structures," *Journal of Manufacturing Science and Engineering,* Vol. 123, No. 4, 2001, pp. 615-622.

11. Beuth, J.L. and Klingbeil, N.W., "The Role of Process Variables in Laser-Based Direct Metal Solid Freeform Fabrication," *JOM*, September 2001, pp. 36-39.

12. Aggarangsi, P., Beuth, J.L., and Griffith, M.L. "Melt Pool Size and Stress Control for Laser-Based Deposition Near a Free Edge," *Solid Freeform Fabrication Proceedings* (D.L. Bourell, R.H. Crawford, J.J. Beaman, K.L. Wood and H.L. Marcus, eds.), Proc. 2003 Solid Freeform Fabrication Symposium, Austin, August 2003, pp. 196-207.

13. Birnbaum, A.J., Aggarangsi, P. and Beuth, J.L., "Process Scaling and Transient Melt Pool Size Control in Laser-Based Additive Manufacturing Processes," *Solid Freeform Fabrication Proceedings* (D.L. Bourell, R.H. Crawford, J.J. Beaman, K.L. Wood and H.L. Marcus, eds.), Proc. 2003 Solid Freeform Fabrication Symposium, Austin, August 2003, pp. 328-339.

14. Aggarangsi, P., Beuth, J.L., and Gill, D.D., "Transient Changes in Melt Pool Size in Laser Additive Manufacturing Processes," *Solid Freeform Fabrication Proceedings* (D.L. Bourell, R.H. Crawford, J.J. Beaman, K.L. Wood and H.L. Marcus, eds.), Proc. 2004 Solid Freeform Fabrication Symposium, Austin, August 2004, pp. 163-1747.

15. Birnbaum, A.J., Beuth, J.L. and Sears, J.W., "Scaling Effects in Laser-Based Additive Manufacturing Processes," *Solid Freeform Fabrication Proceedings* (D.L. Bourell, R.H. Crawford, J.J. Beaman, K.L. Wood and H.L. Marcus, eds.), Proc. 2004 Solid Freeform Fabrication Symposium, Austin, August 2004, pp. 151-162.

16. Vasinonta, A., Beuth, J.L. and Griffith, M.L., "Process Maps for Controlling Residual Stress and Melt Pool Size in Laser-Based SFF Processes," *Solid Freeform Fabrication Proceedings* (D.L. Bourell, J.J. Beaman, R.H. Crawford, H.L. Marcus and J.W. Barlow, eds.), Proc. 2000 Solid Freeform Fabrication Symposium, Austin, August 2000, pp. 200-208.

17. Vasinonta, A., Beuth, J.L., and Griffith, M.L., "Process Maps for Predicting Residual Stress and Melt Pool Size in the Laser-Based Fabrication of Thin-Walled Structures," accepted to *ASME Journal of Manufacturing Science and Engineerin*g.

18. Boley, B.A. and Weiner, J.H., 1960, *Theory of Thermal Stress*, John Wiley & Sons, Inc., 1960.

19. Peckner, D., Bernstein, I.M., *Handbook of Stainless Steel*, McGraw Hill, 1977.

20. Dobranich, D. and Dykhuizen, R.C., "Scoping Thermal Calculation of the LENS Process," Sandia National Laboratories Internal Report, 1998.

21. *Atlas of Stress-Strain Curves,* ASM, 2002, pp. 184.